ISSN 1846-6168 (Print), ISSN 1848-5588 (Online)
https://doi.org/10.31803/tg-20230912143145

Original scientific paper
Received: 2023-09-12, Accepted: 2024-01-24

Influence of Hydroxyapatite Content on Physical and Rheological Properties of Chitosan-based Scaffold

Luka Dornjak*, Fabio Faraguna, Anamarija Rogina

Abstract: Chitosan-based scaffolds offer significant potential in tissue engineering and regenerative medicine. Whilst exhibiting great bio-regenerative and biocompatible properties, their mechanical properties remain quite poor. The presented research is focused on the modification of macroporous chitosan scaffolds with various amounts of bioactive ceramics (hydroxyapatite) and its influence on the physical and rheological properties of the composite scaffold. Chitosan/hydroxyapatite composite scaffolds with a highly porous microstructure have been prepared by suspending hydroxyapatite (HAp) particles into the chitosan matrix. According to SEM imaging, homogeneous dispersion of the inorganic phase in a chemically-crosslinked chitosan matrix had been achieved. The obtained composite scaffolds exhibited lower swelling capacity with respect to pure chitosan after 24 h of incubation in Hanks' balanced salt solution. Rheological measurements show an increase in storage and loss modulus indicating an improvement in mechanical properties under shear stress. Furthermore, no significant change in loss factor (tanδ) was observed indicating no change in composite viscoelastic properties with an increase in HAp content.

Keywords: chitosan; hydroxyapatite; scaffold; rheological properties

1 INTRODUCTION

Bone is a complex and dynamic tissue that provides mechanical support to the body and plays crucial roles in calcium homeostasis and haematopoiesis [1]. The inorganic phase of bone is primarily composed of calcium phosphates (CaP), predominantly in the form of hydroxyapatite (HAp, $Ca_{10}(PO_4)_6(OH)_2$) which corresponds to 65 - 70% of bone tissue [2]. The organic phase is mainly collagen, a large fibrous protein equivalent to the remaining portion [3, 4]. Collagen is mostly responsible for the elastic resistance of the bone, acting as a matrix for the deposition and growth of mineral salts [2, 5, 6]. Human bone can be divided into strong low-porous (cortical) tissue with high stiffness and soft spongy (trabecular) bone tissue with low strength. The inner part of the bone (trabecular) has a three-dimensional highly porous spongy structure with a pore diameter of 100 - 500 μm allowing for unhindered diffusion of nutrients and metabolic waste through the bone [7, 8].

To aid in the bone recovery process, calcium phosphates such as brushite ($CaHPO_4 \times 2H_2O$), monetite ($CaHPO_4$), tricalcium phosphate ($Ca_3(PO_4)_2$) and hydroxyapatite (HAp) can be used. The interest in these phosphates is due to their biocompatibility, bioactivity, resorbability and chemical similarity to the mineral component found within mammalian bones. However, most attention is put on HAp owing to its thermodynamic stability within body fluids [9, 10].

The first stage in bone tissue engineering begins with the design and fabrication of a porous 3D scaffold. In general, the scaffold should be fabricated from a highly biocompatible material that avoids the possibility of eliciting an immunological or foreign body reaction [11]. Furthermore, the chosen material should be able to degrade and resorb into the body at a controlled rate, matching the rate of specific tissue growth [12]. The incorporation of bioactive ceramics, such as HAp, into a biodegradable polymer matrix could produce bioactive composite materials that mimic natural human bone. A composite material would also improve biocompatibility and hard tissue regeneration owing to the embedded ceramic particles within the polymer matrix [13]. Furthermore, if the 3D scaffold is used as a temporary load-bearing support, the structure should maintain the load without showing fatigue or failure. Therefore, the scaffold should achieve a direct bond with surrounding tissue, and at the same time be completely degradable leaving space for new tissue growth. [12, 14].

One of the most investigated biocompatible and biodegradable polymers for 3D porous scaffolds preparation is a linear polysaccharide chitosan (CHT). It is known for its biocompatible, hydrophilic, non-toxic and biodegradable properties [15, 16]. Chitosan allows for the formation of hydrogels which can be used to create optimal 3D porous scaffolds with suitable microstructure for cell proliferation and differentiation; therefore, it has been applied in cartilage tissue engineering [17, 18], wound healing [9] and bone engineering or orthopaedic applications [19, 20]. Unfortunately, it cannot induce and accelerate bone tissue regeneration [21] and also possesses low mechanical properties due to its hydrogel nature, resulting in poor performance as a load-bearing material [2]. Previous research by Santos et al. [9] describes the dependence of cellular growth on the mechanical properties, more precisely, the elastic modulus of biodegradable materials, where an increase in cell growth can be observed with a modulus close to bladder tissue. Here, the choice of crosslinking then plays a pivotal role in scaffold properties. The option between physical [22] and chemical [23] crosslinking of chitosan can determine the scaffold's *in vivo* behaviour. If chitosan is cross-linked via physical interactions, it can result in "weak gels" with higher degradation ability but lower mechanical properties. The use of a chemical crosslinking agent such as genipin, results in a "strong gel" with higher resistance to degradation and improved mechanical properties [24, 25].

In this work, chemically-crosslinked chitosan scaffolds were modified by different amounts of hydroxyapatite

particles in order to prepare composite scaffolds for bone tissue engineering applications. According to Budiraharjo et al. [26] the addition of HAp supports osteoblast attachment and proliferation as well as osteoblastic differentiation of bone marrow stem cells. Jongwattanapisan et al. [27] further confirmed bioactivity by the formation of an apatite layer on the surface of the scaffold allowing for its *in vivo* osteoinductive behaviour. The incorporation of HAp within the polymeric matrix can likely improve mechanical properties under shear stress, possibly increasing the storage and loss moduli which can then be reflected in the material's ability to withstand higher shear stress when implanted in living organisms [28, 29]. In this work, we investigated the influence of different hydroxyapatite content on the physical and rheological properties of potential bone scaffolds. The CHT/HAp scaffolds were fabricated by thermally induced phase separation and chemically crosslinked using genipin. The rheological test showed that prepared scaffolds act as 'strong gels' when subjected to shear stress, with slightly increased storage modulus when hydroxyapatite was added. Obtained chitosan/hydroxyapatite scaffolds were designed as potential structures for aiding in the restoration of small bone defects with limited load-bearing capabilities.

2 EXPERIMENTAL PART

2.1 Synthesis of Hydroxyapatite

A predetermined amount of calcium carbonate ($CaCO_3$; Lachner, Neratovice, Czech Republic) was added into a 0.5% (v/v) solution of acetic acid (Acetic acid 99.8%; Lachner Neratovice, Czech Republic) and left for 2 hours under vigorous stirring. Then, a specific amount of ammonium dihydrogen phosphate (Lachner, Neratovice, Czech Republic) was added, with respect to the hydroxyapatite molar ratio Ca/P of 1.67. The pH of the solution was then adjusted to 9 using ammonia (Alkaloid Ad Skopje; Skopje, North Macedonia) and left for 24 hours under vigorous stirring at ambient temperature. The obtained precipitate was then filtered, washed with demineralized water until neutral pH and dried at 60 °C.

2.2 Preparation of Composite Scaffolds

Chitosan scaffolds were prepared as follows: CHT (Chitoscience 85/200; Heppe Medical Grade Chitosan) was dissolved in acetic acid 0.5% (v/v) in order to obtain a 1.2% (w/v) chitosan solution. After the solution was filtered, genipin (Cayman Chemical Company; Ann Arbor, MI) (a crosslinking agent) was added to the solution (2% w/w in respect to chitosan) and stirring was resumed for 4 h. Following the process of homogenization, the resulting solution was poured into a 24-well plate and subjected to a 24-hour incubation period at 50 °C to facilitate the crosslinking reaction. The obtained cross-linked hydrogels were subsequently frozen at –22 °C and subjected to a 48-hour lyophilization process using a Kambic LIO-5PLT (Slovenia) freeze-dryer. Afterwards, the dried scaffolds underwent a wash in acetone (T.T.T; Sveta Nedelja, Croatia) to eliminate any potential genipin residues. These samples were labelled as CHT.

Chitosan/hydroxyapatite composite scaffolds were prepared as follows: initially, the chitosan solution was prepared as previously outlined, following, different mass fractions of hydroxyapatite were introduced (10 - 30% wt.) under vigorous stirring for 2 hours. Additional homogenization of the obtained suspension was achieved by using a Sonoplus (Germany) 400 ultrasonic probe (40% amplitude) for 3 min. Subsequently, genipin was added to crosslink the prepared composite suspension, following the earlier described method. The obtained composite scaffolds were denoted as HAp 10, HAp 20 and HAp 30 corresponding to the hydroxyapatite weight ratio in composite scaffold.

2.3 Composite Scaffolds Identification

The prepared materials were analysed using a Bruker Vertex 70 ATR-FTIR spectrometer (Massachusetts, USA) at a resolution of 2 cm^{-1} in a spectral range of 4000 - 400 cm^{-1} with 32 scans set at a temperature of 20 °C.

The mineralogical composition was identified by XRD analysis on a Shimadzu XRD 6000 device (Japan) with CuK_α radiation at a voltage of 40 kV and a current of 30 mA. XRD patterns were obtained in step mode in the range of 2θ angles from 5 to 70 ° with a step of 0.02 ° and a step hold of 0.6 s. The average crystallite size of the prepared powder was calculated on the whole diffraction pattern using the DIFFRAC.SUITE TOPAS V.5.0 software (Bruker, Karlsruhe, Germany). Recommended physically sound crystallite value, volume weighted mean size calculated with the integral breadth-based calculation (Lvol-IB), was reported. The structure of Holly Springs HAp [30] was used as a starting model without the inclusion of CO_3^{2-} in the structure.

The microstructure of composite scaffolds was imaged by scanning electron microscope (SEM) TESCAN Vega3 SEM Easyprobe (Czech Republic) with an electron beam energy of 10 keV. An energy-dispersive X-ray (EDX) spectrometer (Bruker B-Quantax; Massachusetts, USA) connected to the SEM has been used to determine the elemental composition of the scaffolds. Prior to the SEM/EDX analysis, the samples were sputtered with gold and palladium for 90 s.

2.4 Swelling Behaviour

The swelling ability of the composite scaffolds was evaluated in Hanks' balanced salt solution (HBSS, pH 7.4) for 24 h at a constant temperature of 37 °C. After incubation time, samples were delicately collected and washed using demineralized water. The swelling degree (%) was expressed as a weight ratio of the absorbed medium and dry sample.

2.5 Rheological Properties

The storage and loss moduli of hydrogels were performed on a rheometer HR 30 Discovery Hybrid Rheometer (TA Instruments; Delaware, USA). Previously swollen samples were placed in parallel plate geometry (25

mm diameter and 1000 μm gap) and then fixed with a preload force (0.7 N). All measurements were carried out at 37 °C. First, an amplitude sweep test carried out at a constant frequency of 0.2 Hz with a strain range from 0.01 to 100.0% was performed to determine the linear viscoelastic range.

2.6 Statistics

The results are displayed as the mean values ± standard deviation. To assess data differences, a two-way analysis of variance (ANOVA) was conducted, followed by a Tukey *post hoc* test. Any significant distinctions between groups were indicated with an asterisk (*).

3 RESULTS AND DISCUSSION

3.1 FTIR Analysis

Prepared composite scaffolds were identified using ATR-FTIR spectroscopy. As depicted in Fig. 1a, the cross-linked chitosan scaffold exhibited distinctive absorption bands: the region between 3360 and 3289 cm^{-1} showed an overlap of bands, corresponding to the stretching vibrations of hydroxyl and amino groups, as well as their interactions through hydrogen bonding [31]. Additionally, two absorption bands at 2920 and 2863 cm^{-1} were observed, which can be attributed to the symmetric and asymmetric stretching of C–H in the $–CH_2$ group. Further, there were two absorption bands at 1644 - 1641 cm^{-1} and 1557 cm^{-1} [32], which could be attributed to the stretching vibrations of the carbonyl group (amide I) and a combination of N–H and C–N stretching vibrations (amide II) [33]. These bands were a result of the crosslinking reaction between chitosan and genipin. The absorption band ranging from 1547 to 1542 cm^{-1} may be ascribed to the presence of the carboxylic group arising from chitosan acetate salt [34]. Additionally, the absorption bands at 1405, 1375, and 1315 cm^{-1} can correspond to the bending vibrations of $–CH_2$ groups from the pyranose ring, as well as $–CH_3$ groups [35, 36], along with stretching vibrations of the C–N bond (amide III). Moreover, the band at 1150 cm^{-1} corresponds to the asymmetric stretching of the C–O–C bridge [37]. Lastly, the absorption bands at 1061 and 1027 cm^{-1} could correspond to the stretching vibrations of C–O–C and – COH bonds, originating from the crosslinking of chitosan with genipin [38–40].

FTIR spectrum of prepared hydroxyapatite (Fig. 1b) shows characteristic absorption bands: the band overlap at 1021 cm^{-1} is associated with symmetric ν_3-PO_4^{3-} bending, while two bands, observed at 600 and 560 cm^{-1}, could be attributed to asymmetric ν_4-PO_4^{3-} bending [41]. Two absorption bands ranging from 3610 to 3000 cm^{-1} and 1635 cm^{-1} can be attributed to physically bound water [42]. Additionally, absorption bands at 1464, 1450, 1418, 880 and 873 cm^{-1} were detected. According to previous studies [27, 43, 44], observed bands can be associated with carbonate groups incorporated in hydroxyapatite lattice. Generally, absorption bands at 1546, 1456 and 880 cm^{-1} are assigned to ν_3 and ν_2 vibrations of the $–CO_3^{2-}$ group that occupies the position of hydroxyl ions, i.e. A-type substitution. On the other hand, B-type substitution, where carbonate groups replace PO_4^{3-} sites, is usually indicated by the bands at 1465, 1413 and 873 cm^{-1} [45] On the contrary, Ren et al. [46] reported on carbonate signature bands for A-type and B-type substitution. The authors concluded that bands at 1450, 1413 and 880 cm^{-1} can be a result of carbonate adsorbed on the apatite crystal surface. Our FTIR results indicate carbonated hydroxyapatite with B-type substitution.

FTIR spectra of CHT/HAp scaffolds (Fig. 1) show the superposition of the chitosan-genipin matrix and HAp spectra; however, some bands are difficult to observe due to band overlap. Furthermore, slight changes in FTIR spectra can be observed with the addition of hydroxyapatite into the chitosan-genipin matrix (Tab. 1). In the composite spectra, a subtle shift in the absorption bands related to phosphate groups can be found, along with a reduction in the intensity of the band corresponding to the C–O–C bond of chitosan. According to El-Sayed et al., [47] such shifts in absorption bands may be attributed to CHT/HAp interaction between chitosan functional groups and phosphate groups of HAp.

Table 1 FTIR absorption bands characteristic of hydroxyapatite.

	Wavenumber, cm^{-1}	
Sample	ν_3–PO_4^{3-}	ν_4–PO_4^{3-}
CHT	/	/
HAp	1025	600, 560
HAp 10	1020	600, 564
HAp 20	1021	601, 564
HAp 30	1020	602, 563

Furthermore, a decrease in the intensity of absorption band at 1063 cm^{-1} could be attributed to the limiting vibrational space for C–O–C bond as a result of HAp modification [21, 48, 49].

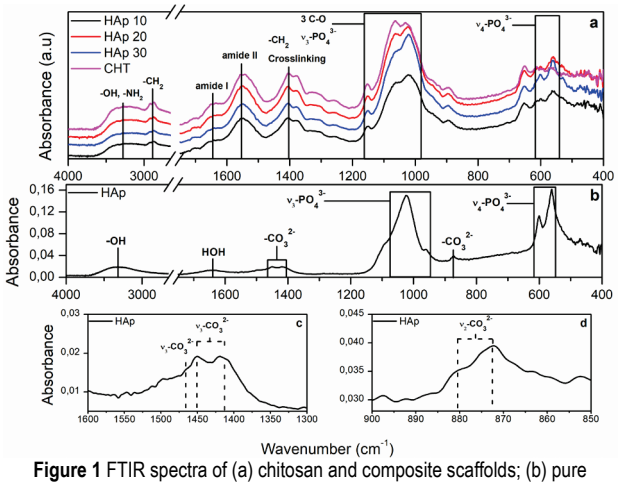

Figure 1 FTIR spectra of (a) chitosan and composite scaffolds; (b) pure hydroxyapatite; detailed view of the (c) 1600-1300 cm^{-1} and (d) 900-850 cm^{-1} FTIR spectra.

3.2 XRD analysis

XRD pattern of synthesized hydroxyapatite is shown in Fig. 2a. For comparison, ICDD data of hydroxyapatite (ICDD 09-432) is given in Fig. 2b. Diffraction maxima at 2θ ~ 25.8°, 28.3°, 32°, 39.6°, 46.6°, 49.4°, 53.2°, 64° corresponding to (002), (200), (211), (310), (222), (213),

(004), (304) reflections of hydroxyapatite confirmed the successful synthesis of HAp through the precipitation method. Moreover, wider diffraction maxima indicated hydroxyapatite of nanometric crystallites with size estimated by Scherrer approximation. The average crystallite size (Lvol-IB) of the prepared powder is 4.9 ± 2.9 nm. It has been reported that nanosized HAp exhibit improved bioresorption *in vitro* and *in vivo* [50, 51].

XRD patterns of composite scaffolds are shown in Fig. 3a. A broad diffraction maximum was detected at $2\theta \approx 21.2°$ which corresponds to the crosslinked chitosan matrix. The addition of HAp into the chitosan matrix resulted in two observable diffraction maxima at $2\theta \approx 25.8°$ (002) and 32° (211) which correspond to the strongest diffraction maxima of HAp [9, 42]. The diffraction maxima at $2\theta \approx 39.6°$ (310), 46.6° (222), 49.4° (213) and 53.2° (004) can also be observed. The presence of HAp diffraction maxima when compared to the diffraction maxima of pure hydroxyapatite (Fig. 3b) indicates the successful incorporation of HAp into the polymeric matrix at a higher HAp weight ratio.

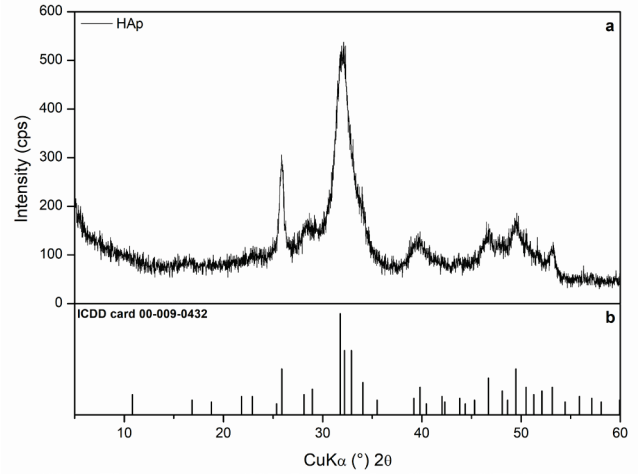

Figure 2 XRD pattern of obtained hydroxyapatite (a) and ICDD data of hydroxyapatite (b)

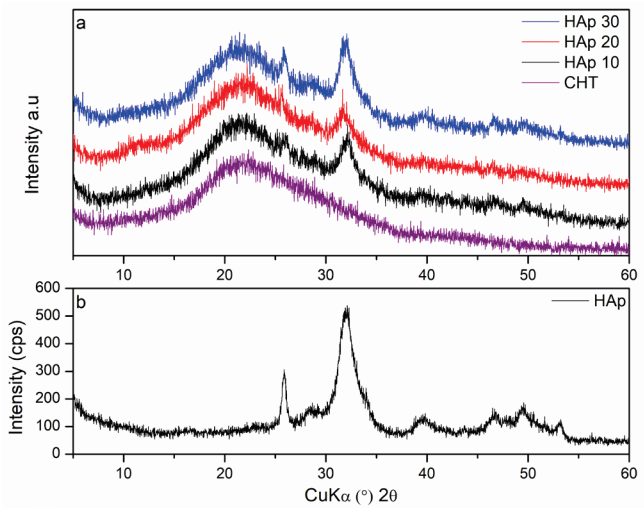

Figure 3 XRD patterns of (a) chitosan and composite scaffolds; (b) pure hydroxyapatite

3.3 Scaffold Microstructure and Elemental Analysis

The microstructure of the obtained composite scaffolds exhibits a high porosity, characterized by interconnected and irregular pores, as depicted in Fig. 4.

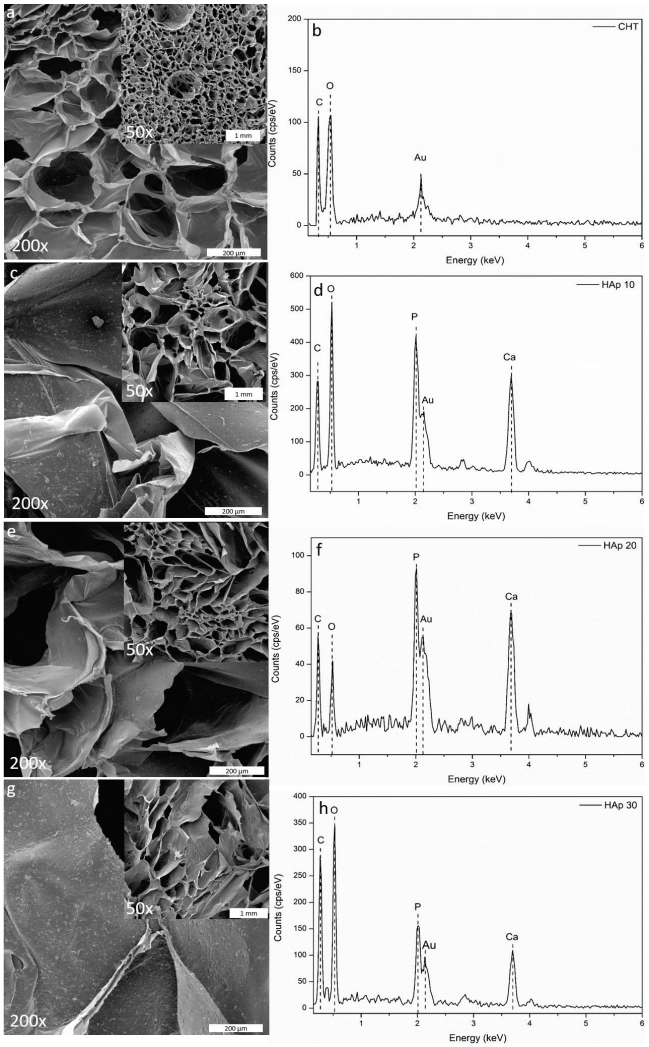

Figure 4 SEM micrographs and EDX spectra of CHT (a, b); HAp 10 (c, d); HAp 20 (e, f); HAp 30 (g, h) scaffold. Scale bar on SEM micrographs: 200 µm and 1 mm.

The crosslinking process is mostly used in order to enhance properties such as stiffness to ensure improved cell adhesion, proliferation and diffusion of nutrients [23, 52]. In this work, genipin was used to produce scaffolds that would be stable under physiological conditions. The samples were first subjected to the process of thermally induced phase separation (TIPS), where a homogeneous polymer solution was frozen, thus creating a multi-phase system with polymer-rich phase and solvent [53]. Next, the system was subjected to the freeze-drying process where nucleated ice crystals from the polymer/solvent system sublimate, thus leaving pores. This process facilitates the formation of a favourable macroporous structure with interconnected porosity, and pore sizes of up to 200 µm, as observed in the crosslinked chitosan scaffold. The addition of hydroxyapatite resulted in the formation of irregular pores of different sizes up to 1 mm. The XRD analysis indicated nanocrystalline hydroxyapatite;

however, nanosized crystals tend to agglomerate forming micrometric particles. Nevertheless, good distribution of HAp agglomerates within the chitosan matrix is observable, especially for composite scaffold with 30% of HAp.

The highly porous nature of the obtained scaffolds is favourable for unhindered resorption of HAp. The composite scaffolds serve as a support during tissue restoration, where porosity, along with pore size, plays a key role in neotissue growth. According to Yang et al., [54] the ideal pore size for cell proliferation and migration falls within the range of 100 to 200 μm; thus, the obtained scaffolds exhibit a microstructure suitable for cell adhesion and tissue growth. Moreover, Oliveira et al. [14] conducted research that shows how the incorporation of hydroxyapatite into composite scaffolds can increase their intractability with bone tissue cells, specifically goat marrow stromal cells (GBMC), by creating a surface substrate through the apatite layer. This substrate facilitates the adhesion of bone tissue cells to the scaffold, thus initiating the process of proliferation and differentiation [55].

The atomic composition of the obtained composite scaffolds was analysed using energy-dispersive X-ray analysis. As seen in Fig. 4. EDX spectra of cross-linked chitosan scaffolds confirm the presence of carbon and oxygen originating from crosslinked chitosan. The EDX spectra of the composite scaffolds indicated the presence of phosphorus at 2.02 keV and calcium at 3.7 keV indicating the presence of CaP phase within the scaffolds, which was identified as hydroxyapatite by XRD analysis.

3.4 Swelling Behaviour

The swelling ratio of the obtained scaffolds was assessed after a 24-hour incubation period in the HBSS buffer, as depicted in Fig. 5. All systems exhibit a high swelling capacity (above 2000%) which could be associated with the hydrophilic hydrogel nature of chitosan and the high porosity of the scaffolds. Although all samples show high swelling values, the addition of hydroxyapatite lowers the swelling capacity of chitosan, especially with an increase in HAp content.

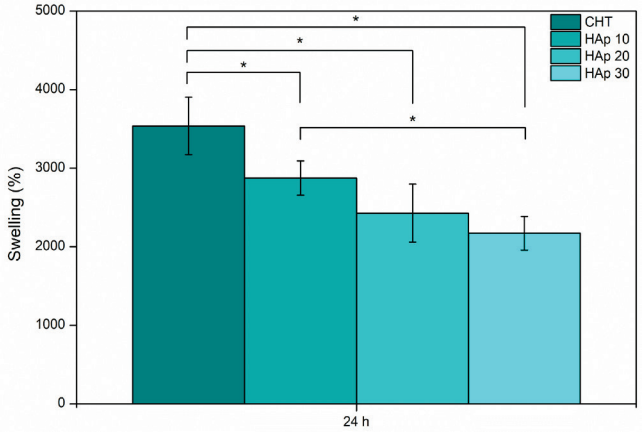

Figure 5 Swelling capacity of chitosan and composite scaffolds in HBSS buffer (pH = 7.4). The significant difference between the two groups is denoted by an asterisk (*) with $p < 0.05$.

According to Ying et al. [56] the decrease can be attributed to a collapse of pores caused by HAp particles. Since such an effect on the microstructure was not observed on SEM micrographs, an effect described by Hu et al. [57] seems to be more likely. They proved that the swelling capacity of chitosan/HAp composites was reduced compared to chitosan due to the formation of a temporary HAp barrier that prevents water from permeating into the chitosan matrix. Furthermore, according to Gupta et al. [58], prolonged exposure of chitosan-based scaffolds to such buffers may result in further degradation of the scaffolds, allowing for an increase in pore size, larger voids between pores and swelling capability. Such a phenomenon may be diminished by the addition of HAp into the polymeric matrix, which has been reported by Tang et al. [59], where a decrease in degradation of the composite can be observed with an increase of HAp content.

The swelling behaviour of scaffolds plays a crucial role in tissue regeneration, allowing for the adsorption and retention of nutrients which in turn creates a cell-nourishing environment capable of sustaining and accelerating cellular regeneration and growth [16, 17].

3.5 Rheological Properties

Polymer hydrogels consist of a polymer network, which can absorb and retain water to form a gel-like structure [60]. The formation is achieved through the process of cross-linking, which results in the formation of a three-dimensional network capable of absorbing and retaining a substantial amount of water or biological fluids (higher than 20%) without disintegration [22, 61].

The existence of cross-links between polymer chains can affect the physical properties of the polymer, depending on the degree of cross-linking and crystallinity. Polymer hydrogels can be divided into two categories, based on the type of crosslinking. "Weak gels" are formed through physical crosslinking, i.e. a crosslinking network obtained through non-covalent interactions, including hydrogen bonding, electrostatic interactions, or van der Waals forces [62–64]. In contrast, chemical crosslinking generates "strong gels" involving the formation of a covalent bond between polymer chains [24, 65]. While physically cross-linked hydrogels are relatively weak and have a reversible swelling capacity, chemical crosslinking results in hydrogels that are stronger and more stable, but typically have less swelling capacity [61]. When it comes to rheological properties (shear modulus), physical and chemical cross-linked hydrogels also display different behaviours. Shear modulus is a measure of the hydrogel's ability to resist deformation under shear stress. Physical hydrogels, with a reversible cross-linking network compared to chemical cross-linking [66], typically exhibit a lower storage modulus (G′, representing the hydrogel's resistance to elastic deformation) and a lower loss modulus (G″, representing the hydrogel's resistance to viscous flow). In contrast, chemical hydrogels, with a more rigid and irreversible cross-linking network, exhibit a higher G′ and a higher G″, indicating a more solid-like behaviour [24, 61, 67, 68].

To determine the rheological properties of the obtained composite scaffolds, first, an amplitude sweep test was used to determine the linear viscoelastic region where shear moduli were independent of oscillatory strain (Fig. 6). As observed, all scaffolds exhibit substantial linear viscoelastic regions (above 20 %) which according to Ross-Murphy et al. [24] is indication of "strong gels" formed by covalent crosslinking agent (genipin) [69]. Furthermore, at strains above 20 % storage modulus starts to decrease ending with an intersection of G′ and G″ lines, indicating a possible collapse of the hydrogel structure. Following the determination of the linear viscoelastic region, the hydrogel storage and loss moduli were evaluated as a function of angular frequency, where the samples were subject to an increasing shear frequency. In comparison to cross-linked chitosan scaffolds, the composite scaffolds (with an exception for HAp 20) show an increase in both storage and loss moduli (Fig. 7) indicating a possible reinforcement of chitosan matrix by HAp particles.

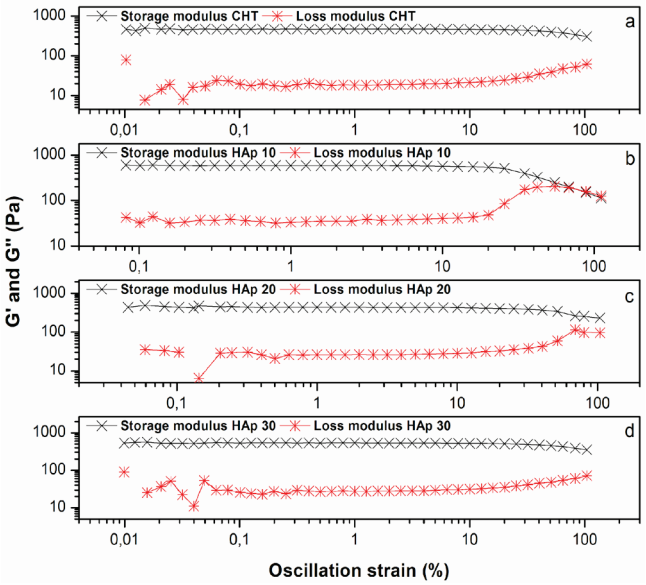

Figure 6 Strain sweep test of composite scaffolds after 24 h of immersion in PBS at a frequency of 0.2 Hz. The G' and G" curves represent the average values of five measurements.

Similar findings have been reported by Demirtas et al. [70] and Ramay et al. [71] on bioprintable chitosan/ hydroxyapatite bio-ink and load-bearing scaffolds for bone regeneration, where a small increase in storage and loss moduli with an increase of hydroxyapatite weight fraction was observed. A significant difference between G′ and G″ was observed with a ratio G″/G′ < 1, additionally confirming the "strong gel" nature of the obtained composite scaffolds [24, 25, 69]. No significant change has been noted in the loss factor value (Tab. 2), indicating no change in the elastic behaviour with HAp addition. Besides composition, swelling capacity and microstructure also affect hydrogels' mechanical properties. As shown, the addition of hydroxyapatite has decreased swelling capacity and caused alteration in pore size and shape which could have an additional effect on improved mechanical properties of composites.

Table 2 Storage modulus (*G'*), loss modulus (*G"*) and loss (damping) factor (tanδ) values for composite scaffolds obtained by frequency sweep.

Sample	Storage modulus *Pa*	Loss modulus *Pa*	tan δ
CHT	412.83 ± 31.77	18.56 ± 2.34	0.04 ± 0.003
HAp 10	658.72 ± 182.82	37.18 ± 8.89	0.05 ± 0.005
HAp 20	495.35 ± 103.88	27.62 ± 6.16	0.05 ± 0.010
HAp 30	672.48 ± 195.42	31.07 ± 5.20	0.05 ± 0.007

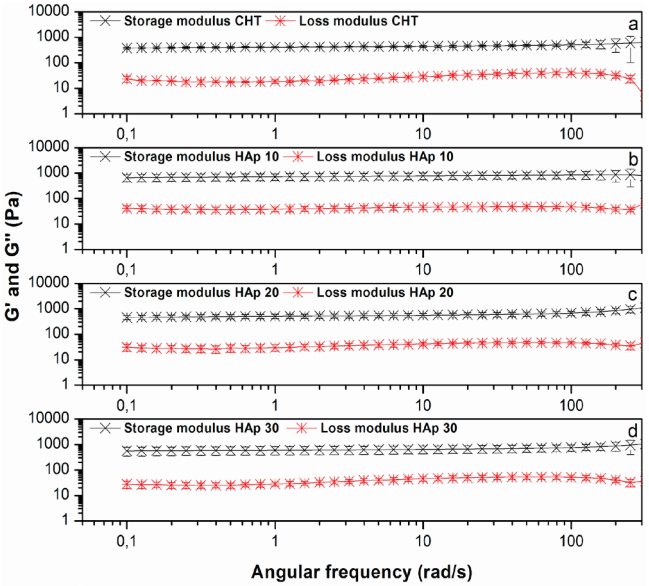

Figure 7 Frequency sweep test of composite scaffolds after 24 h of immersion in PBS at a constant strain of 1%. The G' and G" curves represent the average values of five measurements.

4 CONCLUSION

This work focuses on the synthesis of porous 3D composite scaffolds with improved bioactivity and mechanical properties through modification with bioactive ceramics, hydroxyapatite. The successful synthesis of hydroxyapatite via the precipitation method and HAp incorporation into the chitosan matrix was indicated by XRD, FTIR and EDX analysis. SEM imaging of scaffold morphology indicated the presence of a favourable porous structure with interconnected porosity which combined with the presence of HAp, could act as a good support for cell proliferation and differentiation. The addition of HAp also influenced the swelling properties of the obtained composites, where a decrease in swelling capacity can be observed with an increase in HAp content. Furthermore, rheological characterization indicated a formation of "strong gel" with a slight increase in storage and loss moduli of the composite scaffolds. No significant change in relation to loss factor value indicated no change in viscoelastic behaviour with HAp presence. Such results may indicate a possible slight improvement in the mechanical properties of the composites compared to chitosan scaffolds. Further studies on cytotoxicity will be performed to validate the potential of obtained scaffolds for application in bone tissue regeneration.

Acknowledgment

This work was supported by the Croatian Science Foundation [grant number UIP-2020-02-6201]. The authors thank L. Bauer, PhD from the University of Zagreb for assistance with XRD analysis.

5 REFERENCES

[1] Currey, J. D. (2012). The structure and mechanics of bone. *Journal of Materials Science, 47*(1), 41-54. https://doi.org/10.1007/s10853-011-5914-9

[2] Gomes, D. S., Santos, A. M. C., Neves, G. A., & Menezes, R. R. (2019). A brief review on hydroxyapatite production and use in biomedicine. *Cerâmica, 65*(374), 282-302. https://doi.org/10.1590/0366-69132019653742706

[3] Sato, K. (2007). Mechanism of Hydroxyapatite Mineralization in Biological Systems(Review). *Journal of the Ceramic Society of Japan, 115*(1338), 124-130. https://doi.org/10.2109/jcersj.115.124

[4] Malmberg, P. & Nygren, H. (2008). Methods for the analysis of the composition of bone tissue, with a focus on imaging mass spectrometry (TOF-SIMS). *Proteomics, 8*(18), 3755-3762. https://doi.org/10.1002/pmic.200800198

[5] Jee, S. S., Kasinath, R. K., DiMasi, E., Kim, Y.-Y., & Gower, L. (2011). Oriented hydroxyapatite in turkey tendon mineralized via the polymer-induced liquid-precursor (PILP) process. *Cryst. Eng. Comm, 13*(6), 2077. https://doi.org/10.1039/c0ce00605j

[6] Iijima, M., Moriwaki, Y., Yamaguchi, R., & Kuboki, Y. (1997). Effect of Solution pH on the Calcium Phosphates Formation and Ionic Diffusion on and through the Collagenous Matrix. *Connective Tissue Research, 36*(2), 73-83. https://doi.org/10.3109/03008209709160215

[7] Liu, Y., Luo, D., & Wang, T. (2016). Hierarchical Structures of Bone and Bioinspired Bone Tissue Engineering. *Small, 12*(34), 4611-4632. https://doi.org/10.1002/smll.201600626

[8] Novitskaya, E., Chen, P.-Y., Lee, S., Castro-Ceseña, A., Hirata, G., Lubarda, V. A., & McKittrick, J. (2011). Anisotropy in the compressive mechanical properties of bovine cortical bone and the mineral and protein constituents. *Acta Biomaterialia, 7*(8), 3170-3177. https://doi.org/10.1016/j.actbio.2011.04.025

[9] Santos, M. H., Oliveira, M. de, Souza, L. P. de F., Mansur, H. S., & Vasconcelos, W. L. (2004). Synthesis control and characterization of hydroxyapatite prepared by wet precipitation process. *Materials Research, 7*(4), 625-630. https://doi.org/10.1590/S1516-14392004000400017

[10] Dorozhkin, S. V. (2011). Calcium orthophosphates. *Biomatter, 1*(2), 121-164. https://doi.org/10.4161/biom.18790

[11] Dhandayuthapani, B., Yoshida, Y., Maekawa, T., & Kumar, D. S. (2011). Polymeric Scaffolds in Tissue Engineering Application: A Review. *International Journal of Polymer Science, 2011*(ii), 1-19. https://doi.org/10.1155/2011/290602

[12] Hutmacher, D. W. (2000). Scaffolds in tissue engineering bone and cartilage. In *The Biomaterials: Silver Jubilee Compendium* (Vol. 21, pp. 175-189). Elsevier. https://doi.org/10.1016/B978-008045154-1.50021-6

[13] Stark, G. B., Horch, R., & Táczos, E. (Eds.). (1998). Biological Matrices and Tissue Reconstruction. *Biological Matrices and Tissue Reconstruction*. Berlin, Heidelberg: Springer Berlin Heidelberg. https://doi.org/10.1007/978-3-642-60309-9

[14] Oliveira, J. M., Rodrigues, M. T., Silva, S. S., Malafaya, P. B., Gomes, M. E., Viegas, C. A., … Reis, R. L. (2006). Novel hydroxyapatite/chitosan bilayered scaffold for osteochondral tissue-engineering applications: Scaffold design and its performance when seeded with goat bone marrow stromal cells. *Biomaterials, 27*(36), 6123-6137. https://doi.org/10.1016/j.biomaterials.2006.07.034

[15] Prusty, K. & Swain, S. K. (2019). Chitosan-Based Nanobiocomposites for Wound-Healing Applications. In *Nanostructured Polymer Composites for Biomedical Applications* (pp. 295-314). Elsevier. https://doi.org/10.1016/B978-0-12-816771-7.00015-6

[16] Yang, B., Li, X., Shi, S., Kong, X., Guo, G., Huang, M., … Qian, Z. (2010). Preparation and characterization of a novel chitosan scaffold. *Carbohydrate Polymers, 80*(3), 860-865. https://doi.org/10.1016/j.carbpol.2009.12.044

[17] Madihally, S. V. & Matthew, H. W. T. (1999). Porous chitosan scaffolds for tissue engineering. *Biomaterials, 20*(12), 1133-1142. https://doi.org/10.1016/S0142-9612(99)00011-3

[18] Hutmacher, D. W. (2000). Scaffolds in tissue engineering bone and cartilage. *Biomaterials, 21*(24), 2529-2543. https://doi.org/10.1016/S0142-9612(00)00121-6

[19] Li, Z., Ramay, H. R., Hauch, K. D., Xiao, D., & Zhang, M. (2005). Chitosan–alginate hybrid scaffolds for bone tissue engineering. *Biomaterials, 26*(18), 3919-3928. https://doi.org/10.1016/j.biomaterials.2004.09.062

[20] Venkatesan, J. & Kim, S.-K. (2010). Chitosan Composites for Bone Tissue Engineering—An Overview. *Marine Drugs, 8*(8), 2252-2266. https://doi.org/10.3390/md8082252

[21] Nazeer, M. A., Yilgör, E., & Yilgör, I. (2017). Intercalated chitosan/hydroxyapatite nanocomposites: Promising materials for bone tissue engineering applications. *Carbohydrate Polymers, 175*, 38-46. https://doi.org/10.1016/j.carbpol.2017.07.054

[22] Pita-López, M. L., Fletes-Vargas, G., Espinosa-Andrews, H., & Rodríguez-Rodríguez, R. (2021). Physically cross-linked chitosan-based hydrogels for tissue engineering applications: A state-of-the-art review. *European Polymer Journal, 145*(July 2020), 110176. https://doi.org/10.1016/j.eurpolymj.2020.110176

[23] Muzzarelli, R. A. A. (2009). Genipin-crosslinked chitosan hydrogels as biomedical and pharmaceutical aids. *Carbohydrate Polymers, 77*(1), 1-9. https://doi.org/10.1016/j.carbpol.2009.01.016

[24] Ross-Murphy, S. B. & Shatwell, K. P. (1993). Polysaccharide strong and weak gels. *Biorheology, 30*(3-4), 217-227. https://doi.org/10.3233/BIR-1993-303-407

[25] Picout, D. R. & Ross-Murphy, S. B. (2003). Rheology of Biopolymer Solutions and Gels. *The Scientific World Journal, 3*, 105-121. https://doi.org/10.1100/tsw.2003.15

[26] Budiraharjo, R., Neoh, K. G., & Kang, E. T. (2012). Hydroxyapatite-coated carboxymethyl chitosan scaffolds for promoting osteoblast and stem cell differentiation. *Journal of Colloid and Interface Science, 366*(1), 224-232. https://doi.org/10.1016/j.jcis.2011.09.072

[27] Jongwattanapisan, P., Charoenphandhu, N., Krishnamra, N., Thongbunchoo, J., Tang, I.-M., Hoonsawat, R., … Pon-On, W. (2011). In vitro study of the SBF and osteoblast-like cells on hydroxyapatite/chitosan–silica nanocomposite. *Materials Science and Engineering: C, 31*(2), 290-299. https://doi.org/10.1016/j.msec.2010.09.009

[28] Kumar, B. Y. S., Isloor, A. M., Perisamy, K., & Kumar, G. C. M. (2020). Structure and rheology of chitosan-nanohydroxyapatite composite hydrogel for soft tissue regeneration. In *AIP Conference Proceedings, 2247*, p. 040017. https://doi.org/10.1063/5.0003867

[29] Pighinelli, L. & Kucharska, M. (2013). Chitosan–hydroxyapatite composites. *Carbohydrate Polymers, 93*(1), 256-262. https://doi.org/10.1016/j.carbpol.2012.06.004

[30] Sudarsanan, K. & Young, R. A. (1969). Significant precision in crystal structural details. Holly Springs hydroxyapatite. *Acta Crystallographica Section B Structural Crystallography and Crystal Chemistry, 25*(8), 1534-1543. https://doi.org/10.1107/s0567740869004298

[31] Ren, L., Xu, J., Zhang, Y., Zhou, J., Chen, D., & Chang, Z. (2019). Preparation and characterization of porous chitosan microspheres and adsorption performance for hexavalent chromium. *International Journal of Biological Macromolecules, 135*, 898-906. https://doi.org/10.1016/j.ijbiomac.2019.06.007

[32] Klein, M. P., Hackenhaar, C. R., Lorenzoni, A. S. G., Rodrigues, R. C., Costa, T. M. H., Ninow, J. L., & Hertz, P. F. (2016). Chitosan crosslinked with genipin as support matrix for application in food process: Support characterization and β-d-galactosidase immobilization. *Carbohydrate Polymers, 137*, 184-190. https://doi.org/10.1016/j.carbpol.2015.10.069

[33] Lončarević, A., Ivanković, M., & Rogina, A. (2021). Electrosprayed Chitosan–Copper Complex Microspheres with Uniform Size. *Materials, 14*(19), 5630. https://doi.org/10.3390/ma14195630

[34] Butler, M. F., Ng, Y.-F., & Pudney, P. D. A. (2003). Mechanism and kinetics of the crosslinking reaction between biopolymers containing primary amine groups and genipin. *Journal of Polymer Science Part A: Polymer Chemistry, 41*(24), 3941-3953. https://doi.org/10.1002/pola.10960

[35] Duarte, M., Ferreira, M., Marvão, M., & Rocha, J. (2002). An optimised method to determine the degree of acetylation of chitin and chitosan by FTIR spectroscopy. *International Journal of Biological Macromolecules, 31*(1-3), 1-8. https://doi.org/10.1016/S0141-8130(02)00039-9

[36] Amaral, I. F., Lamghari, M., Sousa, S. R., Sampaio, P., & Barbosa, M. A. (2005). Rat bone marrow stromal cell osteogenic differentiation and fibronectin adsorption on chitosan membranes: The effect of the degree of acetylation. *Journal of Biomedical Materials Research Part A, 75A*(2), 387-397. https://doi.org/10.1002/jbm.a.30436

[37] Fernandes Queiroz, M., Melo, K., Sabry, D., Sassaki, G., & Rocha, H. (2014). Does the Use of Chitosan Contribute to Oxalate Kidney Stone Formation? *Marine Drugs, 13*(1), 141-158. https://doi.org/10.3390/md13010141

[38] Vandevelde, K., & Kiekens, P. (2004). Structure analysis and degree of substitution of chitin, chitosan and dibutyrylchitin by FT-IR spectroscopy and solid state C NMR. *Carbohydrate Polymers, 58*(4), 409-416. https://doi.org/10.1016/j.carbpol.2004.08.004

[39] Yasmeen, S., Kabiraz, M., Saha, B., Qadir, M., Gafur, M., & Masum, S. (2016). Chromium (VI) Ions Removal from Tannery Effluent using Chitosan-Microcrystalline Cellulose Composite as Adsorbent. *International Research Journal of Pure and Applied Chemistry, 10*(4), 1-14. https://doi.org/10.9734/IRJPAC/2016/23315

[40] Mukherjee, D., Azamthulla, M., Santhosh, S., Dath, G., Ghosh, A., Natholia, R., …, Muzammil, K. M. (2018). Development and characterization of chitosan-based hydrogels as wound dressing materials. *Journal of Drug Delivery Science and Technology, 46*, 498-510. https://doi.org/10.1016/j.jddst.2018.06.008

[41] Afshar, A., Ghorbani, M., Ehsani, N., Saeri, M., & Sorrell, C. (2003). Some important factors in the wet precipitation process of hydroxyapatite. *Materials & Design, 24*(3), 197-202. https://doi.org/10.1016/S0261-3069(03)00003-7

[42] Mobasherpour, I., Heshajin, M. S., Kazemzadeh, A., & Zakeri, M. (2007). Synthesis of nanocrystalline hydroxyapatite by using precipitation method. *Journal of Alloys and Compounds, 430*(1-2), 330-333. https://doi.org/10.1016/j.jallcom.2006.05.018

[43] Ślósarczyk, A., Paszkiewicz, Z., & Paluszkiewicz, C. (2005). FTIR and XRD evaluation of carbonated hydroxyapatite powders synthesized by wet methods. *Journal of Molecular Structure*, 744-747(SPEC. ISS.), 657-661. https://doi.org/10.1016/j.molstruc.2004.11.078

[44] Tkalčec, E., Popović, J., Orlić, S., Milardović, S., & Ivanković, H. (2014). Hydrothermal synthesis and thermal evolution of carbonate- fluorhydroxyapatite scaffold from cuttlefish bones. *Materials Science and Engineering C, 42*, 578-586. https://doi.org/10.1016/j.msec.2014.05.079

[45] Bauer, L., Antunović, M., Ivanković, H., & Ivanković, M. (2024). Biomimetic Scaffolds Based on Mn^{2+}-, Mg^{2+}-, and Sr^{2+}-Substituted Calcium Phosphates Derived from Natural Sources and Polycaprolactone. *Biomimetics, 9*(1), 30. https://doi.org/10.3390/biomimetics9010030

[46] Ren, F., Ding, Y., & Leng, Y. (2014). Infrared spectroscopic characterization of carbonated apatite: A combined experimental and computational study. *Journal of Biomedical Materials Research - Part A, 102*(2), 496-505. https://doi.org/10.1002/jbm.a.34720

[47] El-Sayed, E.-S. M., Omar, A., Ibrahim, M., & Abdel-Fattah, W. I. (2009). On the Structural Analysis and Electronic Properties of Chitosan/Hydroxyapatite Interaction. *Journal of Computational and Theoretical Nanoscience, 6*(7), 1663-1669. https://doi.org/10.1166/jctn.2009.1228

[48] Zhang, J., Nie, J., Zhang, Q., Li, Y., Wang, Z., & Hu, Q. (2014). Preparation and characterization of bionic bone structure chitosan/hydroxyapatite scaffold for bone tissue engineering. *Journal of Biomaterials Science, Polymer Edition, 25*(1), 61-74. https://doi.org/10.1080/09205063.2013.836950

[49] Chen, F., Wang, Z.-C., & Lin, C.-J. (2002). Preparation and characterization of nano-sized hydroxyapatite particles and hydroxyapatite/chitosan nano-composite for use in biomedical materials. *Materials Letters, 57*(4), 858-861. https://doi.org/10.1016/S0167-577X(02)00885-6

[50] Shi, D., Jiang, G., & Bauer, J. (2002). The effect of structural characteristics on the in vitro bioactivity of hydroxyapatite. *Journal of Biomedical Materials Research, 63*(1), 71-78. https://doi.org/10.1002/jbm.10087

[51] Matsumoto, T., Tamine, K., Kagawa, R., Hamada, Y., Okazaki, M., & Takahashi, J. (2006). Different Behavior of Implanted Hydroxyapatite Depending on Morphology, Size and Crystallinity. *Journal of the Ceramic Society of Japan, 114*(1333), 760-762. https://doi.org/10.2109/jcersj.114.760

[52] Muzzarelli, R., El Mehtedi, M., Bottegoni, C., Aquili, A., & Gigante, A. (2015). Genipin-Crosslinked Chitosan Gels and Scaffolds for Tissue Engineering and Regeneration of Cartilage and Bone. *Marine Drugs, 13*(12), 7314-7338. https://doi.org/10.3390/md13127068

[53] Conoscenti, G., Carrubba, V. La, & Brucato, V. (2017). A Versatile Technique to Produce Porous Polymeric Scaffolds: The Thermally Induced Phase Separation (TIPS) Method. *Archives in Chemical Research, 01*(02), 10-12. https://doi.org/10.21767/2572-4657.100012

[54] Yang, S., Leong, K.-F., Du, Z., & Chua, C. (2001). The Design of Scaffolds for Use in Tissue Engineering. Part I. Traditional Factors. *Tissue Engineering, 7*(6), 679-689. https://doi.org/10.1089/107632701753337645

[55] Thein-Han, W. W. & Misra, R. D. K. (2009). Biomimetic chitosan–nanohydroxyapatite composite scaffolds for bone tissue engineering. *Acta Biomaterialia, 5*(4), 1182-1197. https://doi.org/10.1016/j.actbio.2008.11.025

[56] Ying, R., Wang, H., Sun, R., & Chen, K. (2020). Preparation and properties of a highly dispersed nano-hydroxyapatite colloid used as a reinforcing filler for chitosan. *Materials Science and Engineering: C, 110*(October 2019), 110689. https://doi.org/10.1016/j.msec.2020.110689
[57] Hu, Q. (2004). Preparation and characterization of biodegradable chitosan/hydroxyapatite nanocomposite rods via in situ hybridization: a potential material as internal fixation of bone fracture. *Biomaterials, 25*(5), 779-785. https://doi.org/10.1016/S0142-9612(03)00582-9
[58] Gupta, K. C. & Jabrail, F. H. (2007). Glutaraldehyde cross-linked chitosan microspheres for controlled release of centchroman. *Carbohydrate Research, 342*(15), 2244-2252. https://doi.org/10.1016/j.carres.2007.06.009
[59] Tang, S., Jiang, L., Jiang, Z., Ma, Y., Zhang, Y., & Su, S. (2023). Improving the mechanical, degradation properties and biocompatibility of nano-hydroxyapatite/chitosan composite scaffold by the introduction of carboxylated bamboo fiber. *Cellulose, 30*(3), 1585-1597. https://doi.org/10.1007/s10570-022-05001-x
[60] Peppas, N. A. & Langer, R. (1994). New Challenges in Biomaterials. *Science, 263*(5154), 1715-1720. https://doi.org/10.1126/science.8134835
[61] Hoffman, A. S. (2012). Hydrogels for biomedical applications. *Advanced Drug Delivery Reviews, 64*(SUPPL.), 18-23. https://doi.org/10.1016/j.addr.2012.09.010
[62] Nguyen, K. T. & West, J. L. (2002). Photopolymerizable hydrogels for tissue engineering applications. *Biomaterials, 23*(22), 4307-4314. https://doi.org/10.1016/S0142-9612(02)00175-8
[63] Maitra, J. & Shukla, V. K. (2014). Cross-linking in Hydrogels - A Review. *American Journal of Polymer Science, 4*(2), 25-31. https://doi.org/10.5923/j.ajps.20140402.01
[64] Aly, A. S. (1998). Self-dissolving chitosan, I. Preparation, characterization and evaluation for drug delivery system. *Die Angewandte Makromolekulare Chemie, 259*(1), 13-18. https://doi.org/10.1002/(SICI)1522-9505(19981001)259:1<13::AID-APMC13>3.0.CO;2-T
[65] Connell, J. J. (1975). The role of formaldehyde as a protein crosslinking agent acting during the frozen storage of cod. *Journal of the Science of Food and Agriculture, 26*(12), 1925-1929. https://doi.org/10.1002/jsfa.2740261216
[66] Bawa, P., Pillay, V., Choonara, Y. E., & du Toit, L. C. (2009). Stimuli-responsive polymers and their applications in drug delivery. *Biomedical Materials, 4*(2), 022001. https://doi.org/10.1088/1748-6041/4/2/022001
[67] Shaw, M. T. (2011). *Introduction to Polymer Rheology*. Hoboken, NJ, USA: John Wiley & Sons, Inc. https://doi.org/10.1002/9781118170229
[68] Annabi, N., Tamayol, A., Uquillas, J. A., Akbari, M., Bertassoni, L. E., Cha, C., … Khademhosseini, A. (2014). 25th Anniversary Article: Rational Design and Applications of Hydrogels in Regenerative Medicine. *Advanced Materials, 26*(1), 85-124. https://doi.org/10.1002/adma.201303233
[69] Almdal, K., Dyre, J., Hvidt, S., & Kramer, O. (1993). Towards a phenomenological definition of the term 'gel.' *Polymer Gels and Networks, 1*(1), 5-17. https://doi.org/10.1016/0966-7822(93)90020-I
[70] Demirtaş, T. T., Irmak, G., & Gümüşderelioğlu, M. (2017). A bioprintable form of chitosan hydrogel for bone tissue engineering. *Biofabrication, 9*(3), 035003. https://doi.org/10.1088/1758-5090/aa7b1d
[71] Ramay, H. R. R., & Zhang, M. (2004). Biphasic calcium phosphate nanocomposite porous scaffolds for load-bearing bone tissue engineering. *Biomaterials, 25*(21), 5171-5180. https://doi.org/10.1016/j.biomaterials.2003.12.023

Authors' contacts:

Luka Dornjak, mag. chem.
(Corresponding author)
University of Zagreb, Faculty of Chemical Engineering and Technology,
Trg Marka Marulića 19, 10000 Zagreb, Croatia
ldornjak@fkit.unizg.hr

Fabio Faraguna, Assoc. Prof.
University of Zagreb, Faculty of Chemical Engineering and Technology,
Trg Marka Marulića 19, 10000 Zagreb, Croatia
ffaraguna@fkit.unizg.hr

Anamarija Rogina, Assoc. Prof.
University of Zagreb, Faculty of Chemical Engineering and Technology,
Trg Marka Marulića 19, 10000 Zagreb, Croatia
arogina@fkit.unizg.hr